Electrically Tunable Open-Stub Bandpass Filters Based on Nematic Liquid Crystals

E. C. Economou,[1,*] J. Lovejoy,[1] I. Harward,[1] J. E. Nobles,[1] P. Kula,[2] J. Herman,[2] A. Glushchenko,[1] and Z. Celinski[1]

[1]*Department of Physics and Energy Science, University of Colorado at Colorado Springs, Colorado Springs, Colorado 80918, USA*

[2]*Institute of Chemistry, Military University of Technology, Warsaw 00-908, Poland*

(Received 13 July 2017; revised manuscript received 5 October 2017; published 12 December 2017)

Electrically tunable bandpass filters based on liquid crystals are designed, built, and characterized using a vector network analyzer. The filters are composed of half-wavelength open stubs and quarter-wavelength connecting lines in an inverted microstrip geometry. The filters are modeled using computational electromagnetics software utilizing the finite integration technique. Photolithography and thin-film deposition processes are employed, and standard liquid-crystal cell-assembly techniques are used to make the final filter structures. The three-stub filters with passband central frequencies of 30, 50, and 85 GHz are filled with the nematic liquid crystal, LC1917, and tested. 10% tuning of the central frequency is achieved with a 14-volt peak-to-peak ac bias across the 38-μm liquid-crystal layer (electric field of 0.19 V/μm). At 50 GHz, the insertion loss is −3.76 dB, while the return loss ranges from −9 to −25 dB, indicating a good impedance match for a proof-of-concept device. The passband widths of the 30-, 50-, and 85-GHz filters are 5, 9, and 14 GHz, respectively, resulting in a Q factor of 6. The filter devices presented in this study, although intended for microwave signal-processing applications, furnish an effective methodology for characterizing the dielectric properties of liquid-crystal materials (and fluids or solids in general) up to the terahertz frequency range.

DOI: 10.1103/PhysRevApplied.8.064012

I. INTRODUCTION

There has been an increasingly strong demand for microwave and millimeter wave signal-processing devices operating in the frequency range from 1 to 300 GHz. This trend has grown for many reasons. Higher frequencies allow, for example, far more bandwidth, enhanced line-of-sight propagation, reduced size, and lower costs [1]. In microwave or millimeter wave systems, waveguides and planar transmission-line structures such as slot lines or microstrips are typically used. For planar structures, tunable bandpass filters embedded into transmission lines are of particular interest.

A bandpass filter is a two-port device that provides transmission in a small range of frequencies known as the passband, while attenuating all other frequencies [1]. Tuning of the passband frequency is typically accomplished by using ferroelectrics, ferrites, garnets or spinels, or microelectromechanical systems [2]. However, some of these materials or methods have various disadvantages, including high power consumption, size, cost, low reliability, or limiting operational frequency. One of the recent developments that addresses these problems is the use of liquid crystal (LC) in microwave devices [3–9].

The dielectric constant in LC materials, sensed by the electromagnetic radiation propagating through the medium, changes between $\epsilon_{\parallel}$ and $\epsilon_{\perp}$ and is associated with orientation of the LC molecules with respect to the electric field direction. This orientation can be controlled in an analog manner by applying an electric field across a thin film of LC confined between two surfaces. The permittivity $\epsilon_{\perp}$ corresponds to the case where the LC molecules are aligned with the surface (accomplished using a thin film of rubbed polyimide that anchors the LC molecules to the surface). By applying an ac bias voltage across the LC layer, the nematic director (direction of average orientation of the LC molecules) can be rotated to an alignment parallel with the electric field. In this case, the permittivity is denoted as $\epsilon_{\parallel}$. Electromagnetic waves propagating through the LC medium sense a different orientation of the molecules (due to applied ac bias), thereby changing the propagating signal's wavelength. Such behavior can be utilized to tune the passband frequency of a microwave filter. However, first one needs to determine the properties of LC in gigahertz frequencies which in itself represents a challenge.

Measurement of the frequency-dependent dielectric properties of LCs is well established for the visible range or for frequencies below 1 MHz [10]. In contrast, there is no standard method for this measurement in the 1–1000-GHz range. There are a number of fundamental issues associated with this frequency range. First, bulklike measurements (cavity based) at lower frequencies require large amounts of material (1 cm^3), which is not appropriate for large-scale testing of rare materials [11–12]. In the

*Corresponding author.
evangelos42@gmail.com

250-GHz to 1-THz range one can use infrared spectroscopy schemes, but this still requires up to 200 mm^3 of material [13].

While in this paper we concentrate our attention on the development of bandpass filters in the millimeter wave frequency range we also describe how developed structures can be employed to determine the properties of LC in gigahertz frequencies, especially the dispersion relation and losses. The alternative metrology involves using resonance structures embedded in microstrip waveguides that together with a vector network analyzer (VNA) allows, in principle, the characterization of LC materials up to 750 GHz. We note that in our paper we demonstrate properties of particular LC materials up to 110 GHz due to the used equipment. Furthermore, the ultrasmall waveguides significantly concentrate the energy of the input wave, creating oscillating electric fields with an amplitude on the order of 1 $V/\mu m$. This allows one to probe both the linear and *nonlinear* dielectric coefficients at these frequencies. Therefore, these structures may be used to explore alternative physics and, as a result, high power applications of these materials could emerge. Finally, nearly all LC materials are developed keeping in mind applications in visible or near-infrared frequencies. This means that LC material properties are not optimized for gigahertz frequencies. Currently, one simply selects LC material from existing ones and tries to utilize its properties in a completely different spectrum of electromagnetic frequencies for which the material is developed. Because of the small size of our structures, the estimated volume of LC material used is only 1–2 mm^3, which is a factor of at least 100 times less material than what is used in existing methods. This is important because preparing small amounts of many alternative LCs (containing up to 20 different chemical compounds) is feasible and cost effective. Thus, this alternative evaluation method, which makes it possible to rapidly determine LC properties, will allow chemists to choose the optimal path of synthesis for alternative materials with the goal to optimize performance for applications in gigahertz frequencies.

From the point of view of the signal-processing industry, the presented filter devices based on LCs have various advantages over other reconfigurable filters. Compared with filters based on garnets, spinels, or ferrites, which utilize a magnetic field for tunability, the LC filter devices are very lightweight and power efficient as an electric field is used for tuning (typically less than 1 mW of power is required). The ferroelectrics- (e.g., barium strontium titanate) based filters may also be lightweight and power efficient, but their operational frequency is limited typically to 40 GHz [2]. Mechanical methods for tuning (e.g., microelectromechanical systems) are promising because of their low power consumption and wide frequency range of operation, but are sometimes subject to problems like sticking [3]. LC filters, on the other hand, may be tuned with either an electric or magnetic field. They have low inherent losses, large dielectric anisotropy (and therefore tunability), low power consumption, and small size. In addition, LC display manufacturing is a mature industry whose technological processes can be employed immediately for rf applications.

Although LCs are typically designed for visible-light applications, an understanding of the correlation between their molecular structure and behavior in the near-infrared, far-infrared, and millimeter wave frequency range is beginning to develop. Upon synthesizing the materials, their figure of merit parameter relating modulation (related to optical anisotropy) with the absorption and dichroism can be determined to further optimize the molecular structure of the LCs for microwave and millimeter wave applications. Fortunately, the existing molecular structure of the LCs reported in this study makes the LCs largely suitable for these applications.

Tunable LC-based microwave filters have been developed by other research teams in the last few years [3,14–17]. Bernigaud *et al.* [14] have developed a half-wavelength, open-circuited stub resonator using Merck K15 LC. Its central passband frequency was near 10 GHz and was tuned by 100 MHz with a dc voltage. In addition, they developed a dual-behavior resonator filter (a filter with two parallel, open-circuited stubs of different lengths) based on Merck BL037 LC with a central frequency of 5 GHz. It was capable of tuning by 300 MHz and its S_{21} transmission ranged from −4 to −6 dB in the passband region. Structures developed by Torrecilla *et al.* [16] achieved 7.3% tuning of a 5-GHz passband frequency using the Merck MDA-98-1602 LC. It employed a microstrip square-patch resonator with a central square notch. The S_{21} transmission in the passband was approximately −7 dB. Goelden *et al.* [17] designed a three-pole filter at 20 GHz with 10% tuning capability and passband insertion loss of −9 to −11 dB. Finally, three-stub filters based on LC W1825 with passband frequencies of 80 and >110 GHz have been developed by Lovejoy [3]. These filters were tunable by 12% and had a passband insertion loss of −8 dB. The results from these latest mentioned studies motivated us to design LC-based bandpass filters at gigahertz frequencies with (i) greater tuning capacity with ac biasing to extend the operational life, (ii) improved return and insertion loss, (iii) alternative microstrip geometries, and (iv) better control of the bandwidth. The main advantages of the proposed filters compared with prior research are the lower passband insertion loss (−3.76 dB) and small power consumption. In addition, the presented structures can be used to determine the dispersion relation of LC materials over a wide frequency range. This can be accomplished by employing an experimental setup (described in Sec. II F) that implements an ac bias scheme with a VNA and allows one to observe multiple passband resonances (as mentioned above and in Sec. II B).

In this work, the nematic LCs, LC1917 and LC2020, which are modifications of the LC1825 material [18], are used. Both are composed of isothiocyanato-terminated structures, which belong to a different family of LCs, i.e., laterally fluorosubstituted alkyl-oligophenyls (biphenyls, terphenyls), alkyl-tolanes (phenyl-tolanes, biphenyl-tolanes), and alkylcyclohexyl-tolanes [19]. Crystallization temperatures are found to be below 0 °C for both materials. The clearing temperature for LC1917 is higher than LC2020, at 134.1 °C and 103.0 °C, respectively. Although the chemical nature of LC components is similar in LC1917 and LC2020, the materials differ in the number of higher electron conjugated ingredients, resulting in slightly different birefringence values ($\Delta n_{1917} = 0.42$ and $\Delta n_{2020} = 0.45$ at 589 nm).

The time "*on*" of both LCs, defined as the time that it takes an electric field to reorient the LC molecules from planar to homeotropic alignment, is in the range of 2–5 ms (data not shown). The time "*off*" of the LCs, defined as the time it takes for the LC molecules to relax back to planar alignment, however, is approximately 10 s for a 40-μm-thick LC layer. Therefore, the time *off* is the limiting factor in the total switching time of the LC-based devices. If necessary, the time *off* can be reduced by incorporating in-plane switching to reorient the LC molecules, or by using a smaller LC thickness. Since the time *off* is proportional to the square of the LC layer thickness [10], using a thinner LC layer can reduce the reorientation time substantially. Also, using a different class of LC materials such as dual frequency or smectic C^* [10] would reduce the switching time considerably, to a few milliseconds.

In the sections ahead, we report on the development of tunable open-stub filters based on the above-mentioned LCs, with passband frequencies (f_1) centered at 30, 50, and 85 GHz, as well as describe how these structures can also be used to develop novel metrology of this class of materials. In Sec. II we briefly discuss the filter layout, design, fabrication, and LC material characterization. Section III provides a detailed description of filter performance at different frequencies. We also compare CST Microwave Studio simulation results of filters with three, five, and seven stubs. In the conclusion section, we summarize the presented results. We note that this LC material does not have any inherent resonances up to terahertz frequencies; therefore, this LC-based technology can be easily extended to much higher frequencies than the three frequencies we have mentioned above.

II. DEVICE FABRICATION AND CHARACTERIZATION

A. Open-stub filter design

The LC-based devices typically require two physical surfaces (substrates) between which a LC material is confined. Figure 1 shows the basic AUTOCAD layout of a LC cell containing the inverted microstrip filters (designed for $f_1 = 30$ GHz). Shown at the top of the drawing is the LC cell consisting of two substrates: microstrip filters and coplanar waveguide (CPW) structures deposited on the bottom glass (in orange) and the top ground plane (outlined by blue, dashed lines). A LC material is confined between the top and bottom substrates. We discuss below how this geometry can be used to design and construct the LC-based bandpass filters.

An extensive design theory of bandpass filters may be found in the literature [20–21]. The stub filters in this study utilize a cascade of open-circuited, half-wavelength stubs bridged by quarter-wavelength connecting lines (see Fig. 1). In the passband region, electromagnetic waves propagating through the filter undergo constructive interference due to the stubs with $\lambda/2$ length. Starting with the basic equation for constructive interference, the length of an individual stub for a desired passband frequency is determined by

$$L_{\text{stub}} = c/(2f_1\sqrt{\epsilon_{\text{eff}}}), \tag{1}$$

where L_{stub} is the physical length of a stub, c is the speed of light in vacuum, f_1 is the midband frequency of the filter's passband, and ϵ_{eff} is the effective permittivity of the microstrip line with dielectric overlay. The length of a

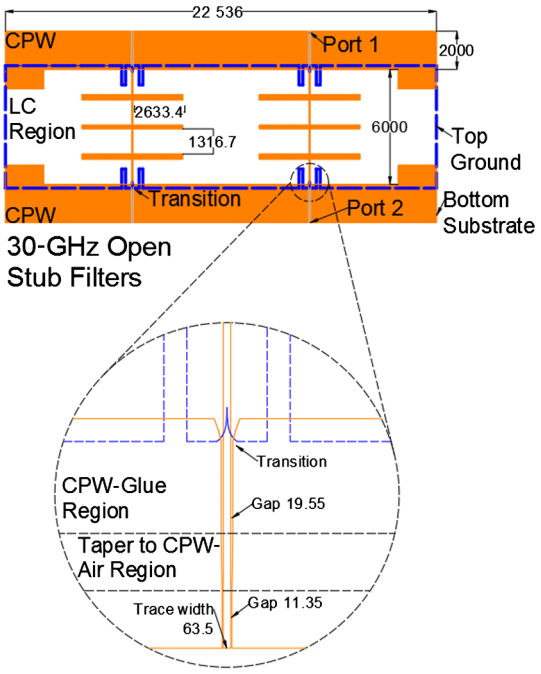

FIG. 1. AUTOCAD rendering showing the basic construction of an LC cell with microstrip filters. The bottom substrate supports the microstrip and CPW elements (in orange). The top substrate (blue, dashed outline) supports the ground plane. A 38-μm-thick LC layer is set between the two substrates. The bottom of the figure shows details of the CPW-to-microstrip transition used to inject the microwave and bias signals. All units are in microns.

connecting line is $L_{cl} = L_{stub}/2$. In addition to the passband frequency, there are secondary passband resonances at integer multiples of f_1. We note that this feature can be employed to determine the permittivity's dispersion relation of studied LC materials. We will discuss in detail in the next subsection how studied structures can be used to develop metrology of LC materials in the gigahertz frequency range. Stopbands are also naturally located at the frequencies $f_1/2$ and $3f_1/2$ and can be adjusted by enforcing a varying admittnce throughout the length of each stub [20].

For the given physical length of the stub, from the above Eq. (1), it is clear that the passband frequency f_1 may be tuned by varying ϵ_{eff} of the microstrip. This is accomplished by applying an electric field across the LC layer, thereby increasing the LC permittivity ϵ_{eff}. This increasing effective permittivity leads to shortening of the signal wavelength relative to the stub's physical length and, consequently, to a decrease in the passband frequency.

B. Metrology of liquid-crystal materials in gigahertz frequencies

As mentioned in the Introduction, LC materials are typically designed and fabricated for the optical or near-infrared frequency spectrum of electromagnetic radiation. However, recently these materials have started to attract attention for applications in gigahertz frequencies, making it necessary to understand their properties in this spectrum range. Below, we outline the procedure that allows us to determine the permittivity of the LC materials as a function of the frequency in designed filter structures. While we present results obtained at room temperature we note that these measurements can be carried out at different temperatures (for example, −55 to 125 °C) by utilizing a temperature stage.

Figure 2 illustrates how filter structures can be used to determine the dielectric properties of LC materials. It depicts the frequency dependence of S parameters, S_{11} (reflection), and S_{21} (transmission). Clearly visible resonances are the first three harmonics associated with a given geometrical length of the open stub. The fourth resonance is just outside of the VNA measuring range (0.05–110 GHz). Using a different VNA setup that allows measurements in a frequency range above 110 GHz would reveal higher harmonics. The resonance frequencies [see Eq. (1)] are only determined by the value of effective permittivity that combines the properties of both substrate and LC materials. To determine permittivity of the LC materials one needs to first know the properties of the substrates as a function of frequency. This can be accomplished by building a filter structure that uses air (instead of LC materials) as a dielectric medium through which electromagnetic waves propagate. In such cases one can determine dispersion relations of the substrate material (in our case, Borofloat 33 glass) because the effective permittivity of the microstrip can be approximated using an analytical formula [22] derived for microstrip lines with multilayered dielectrics under the assumption of quasi-TEM mode propagation or by modeling using, for example, CST software. The determined value of ϵ_{eff} depends on the known permittivity of air (1.000 569 up to 30 GHz [23]—for all practical reasons can be set to 1) as well as the glass permittivity. Knowing permittivity of the substrate as a function of frequency allows one to measure permittivity of LC materials or other materials repeating the above-described procedure.

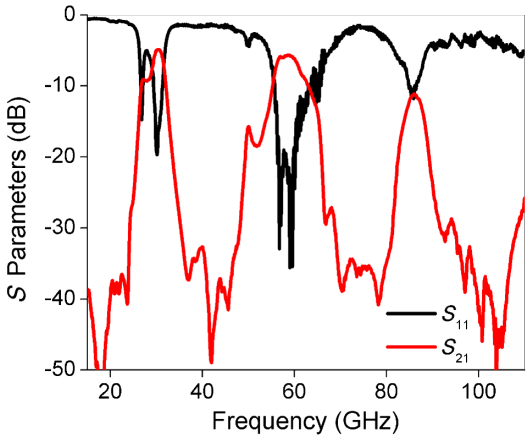

FIG. 2. The measured frequency dependence of S parameters on a three-stub filter structure at room temperature.

We illustrate below how to determine the values of $\epsilon_{\parallel}$ and $\epsilon_{\perp}$ of the LC materials. First, a filter structure with known dimensions is built and the S parameters are measured as a function of frequency (see Sec. II F for measurement details). The observed resonances of both the unbiased and fully saturated LC are then compared with simulations performed on a modeled filter for various values of the LC permittivity. Figure 3 shows how a change in LC permittivity affects the frequency of the first resonance as predicted by CST modeling. This approach allows us to determine the permittivity of LC materials from the measured resonances. Repeating this procedure for higher harmonics allows one to measure a dispersion relation of the measured materials. Building structures with lower fundamental frequency f_1 would provide more experimental data points than the three observed resonances in the currently built structure.

In gigahertz frequencies, $\epsilon_{\perp}$ and $\epsilon_{\parallel}$ of both LCs studied (LC1917 and LC2020 [19,24–25]) are found to be 2.76 and 3.70, respectively ($\Delta\epsilon = 0.940$). We confirm that the LCs are approximately nondispersive by experimentally observing that the second and third passbands are at nearly integral multiples of the fundamental frequency f_1. As mentioned above, this technique can be used also to measure properties of solids. For example, for our work we determine the permittivity of the solid layer of Norland

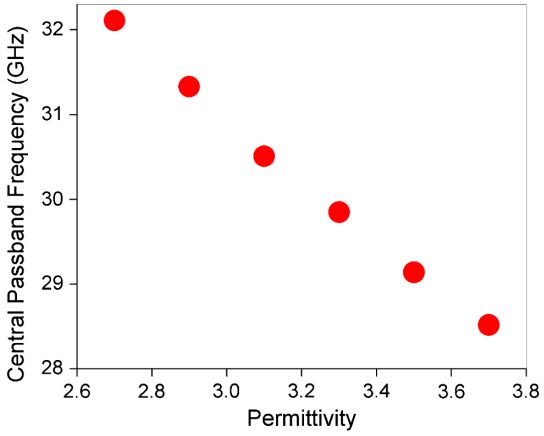

FIG. 3. The frequency of resonances as a function of LC2020 permittivity predicted by CST modeling of a three-stub filter.

Optics glue (NOA68T) that enables us to design the transition from CPW to microstrip geometry as discussed below (result not shown).

C. Determination of stub dimensions for filters with 50-Ω impedance

All LC devices are designed using the mean permittivity value, defined as $\epsilon_c = (\epsilon_\parallel + \epsilon_\perp)/2$, of the LC in order to minimize impedance mismatching as the LC is tuned from its unbiased state to its fully saturated state. These permittivity values of Borofloat 33 and ϵ_c of the LC material are used to determine the stub lengths of the 30-, 50-, and 85-GHz filters employing Eq. (1); the stub length needed to achieve a passband at 30 GHz is 2633 μm (see Fig. 1). The filters with passband frequencies of 50 and 85 GHz (not shown) have stub lengths of 1568 and 922 μm, respectively. The studies of similar LC materials [9] indicates that in the frequency range from 1 to 110 GHz, these LCs are nearly nondispersive (constant group delay).

Finally, the stub widths are determined. The impedances of the individual stubs and connecting lines are first calculated using standard design synthesis equations [20,26] to maintain 50-Ω impedance in the filter structure. CST Microwave Studio is then used to find the stub widths, given these impedances. The widths of the center and outer stubs of all three filters are 194.8 and 275.1 μm, respectively. The connecting linewidth is 59.7 μm.

D. Inverted microstrip and coplanar waveguide design

A CPW to inverted microstrip transition is utilized at the input and output of the filters to effectively inject the microwave and bias signals into the filter structure (see Fig. 1). The copper in the CPW-microstrip structure is 2.25 μm thick. CST simulations are performed to determine the width of a microstrip line necessary to maintain a characteristic impedance of 50 Ω for the center value of LC permittivity ϵ_c. The optimal microstrip width is 63.5 μm. The trace width of the CPW is set to 63.5 μm, and CST simulations are performed to determine the optimal CPW gap width (between signal line to ground). In the CPW-air region, the gap width is 11.4 μm and gradually increases to 19.6 μm in the CPW-glue region (where glue is used to seal the LC cell—see Fig. 1). This value for gap width is determined using the permittivity value of NOA68T glue (3.0 at 30 GHz) obtained with the method described in Sec. II B).

The CPW-microstrip transition region had cutouts in the CPW grounds and the top ground plane based on the geometry presented by Chen *et al.*[27], and other teams [28–29]. This geometry is designed to continuously change the electric field distribution in the transition region between CPW to microstrip, while maintaining an impedance match over a broad bandwidth. Such transitions from CPW to the microstrip significantly improve the performance of our filters when compared with an abrupt transition from CPW to microstrip by about 2–3 dB.

E. Microwave device fabrication

Using photolithography, the filter metallic structures are defined on a glass substrate and copper is deposited by magnetron sputtering. Before photolithography, the 1.1-mm-thick borosilicate glass (Borofloat 33) is cleaned with acetone, isopropyl alcohol (IPA), and deionized water to remove contaminants. Residual solvents are removed by baking. A thin film of negative photoresist (AZ nLOF 2035) is spin coated onto the glass at 2700 RPM for 36 s with a 500 RPM/s initial ramp rate, followed by a 110 °C prebake for 60 s. Using an MJB4 mask aligner (SUSS MicroTec) the metallization pattern is created on glass by exposing a photomask to ultraviolet light for 8 s, followed by a 110 °C postbake for 60 s. Finally, the pattern is developed in AZ 300 MIF developer.

Using magnetron sputtering, a 6–7-nm stainless steel adhesion layer followed by a 2.25-μm copper layer is sputtered onto the substrate. After deposition, the substrate is placed in resist stripper for lift-off leaving the desired copper pattern. The copper ground planes, which serve as the backing of the LC cells, are also prepared using the above-mentioned photolithography and sputtering processes.

The ground plane and substrate with metallic filter structures are put together using LC cell-assembly techniques [30] modified for our purpose. To prepare an alignment layer, a polyimide (1-to-4 solution of RN1744 polyimide-to-no. 21 solvent) is spin coated onto both substrates at 2000 RPM for 30 s and baked at 100 °C under vacuum for 75 min. Vacuum and low temperature is necessary to hinder chemical interaction of the solvent with the copper. After cooldown, the polymer is rubbed mechanically with a rubbing machine equipped with a velvet cloth drum to create an alignment layer that establishes the

unbiased orientation of the LC molecules' direction. Thin, conducting tape is placed between every CPW-microstrip transition in order to bridge the CPW grounds with the microstrip ground plane at the end of the assembly process. Solid glass microspacers are suspended in isopropyl alcohol and spin coated onto one of the substrates at 1400 RPM for 20 s onto one of the substrates. The rubbed substrates are then aligned, glued together with NOA68T photopolymer, and irradiated with ultraviolet light for 2 min. The conducting tape is then soldered to the CPW grounds. Finally, a capillary tube is used to fill the cells with the LC material under vacuum. Figure 4 shows photographs of the front (top) and back (bottom) sides of one of the LC cells with embedded three-stub, 30-GHz filters.

F. Experimental configuration

S-parameter measurements are carried out with a VNA (Agilent Technologies, E8361A) combined with a millimeter head controller (N5260A) and combiner assembly (60012/3) extending characterization up to 110 GHz. Ground-signal-ground probes are used to inject the microwave and ac-bias signals through the two CPW ports on the LC devices. ac biasing of the LC devices is performed with an in-house developed setup that allows the application of variable frequency biasing signals to a VNA [31]. The bias signal from this setup is applied directly through the force-to-ground bias tee on one of the combiner assemblies. The bias signal is a 1-kHz-square wave with an amplitude of applied voltage from 0 to 30 V peak to peak (V p.p.). LabVIEW is used to control the VNA and ac biasing setup and data acquisition. After measurements, on-wafer multiline thru-reflect-line (TRL) calibration is performed using NIST MultiCal software [32].

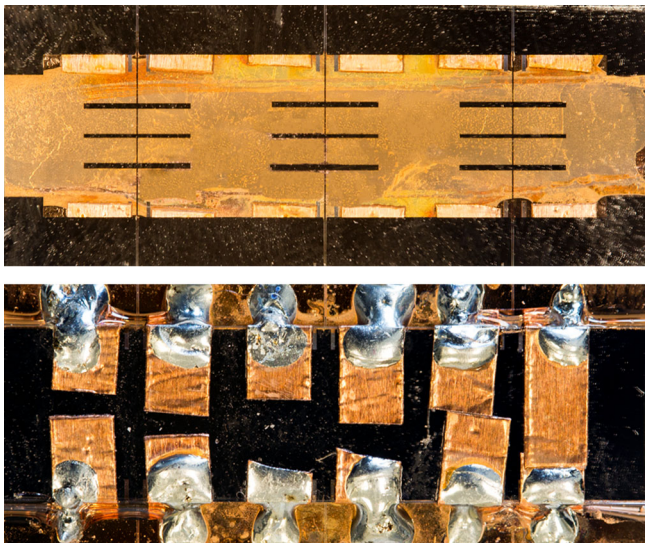

FIG. 4. Photographs showing the front (top) and back (bottom) side of a LC cell with three-stub, 30-GHz filters.

III. RESULTS AND DISCUSSION

A. Analysis of insertion loss due to coplanar waveguide and liquid crystal

Ideally, the passband insertion loss of the filters should be 0 dB, with a return loss of at least −15 dB. However, some insertion loss in the passband region is expected due to the attenuation of the signal propagating through the glass and LC media as well as eddy current losses in the metallic signal lines. To understand the contribution of loss from the CPW on glass, *S*-parameter measurements are performed on CPW structures with different trace lengths. Figure 5 shows a graph of insertion loss S_{21} as a function of frequency for CPWs with lengths of 0.3 cm (black curve), 0.6 cm (red curve), and 1 cm (blue curve). The insertion loss of each CPW is linear in the frequency range from 0 to 95 GHz. As expected, the insertion-loss magnitude increases proportionately with the CPW length as well as the frequency of the propagating wave. At 30 GHz, a 1-cm-long CPW results in −1.8 dB of insertion loss. From these experimental results, we may extrapolate the amount of insertion loss to be expected from the CPW in each filter device. All LC cells presented in this study have 2 mm of CPW on each side. Therefore, the CPW insertion loss expected at 30, 50, and 85 GHz is −0.53, −0.93, and −1.5 dB, respectively.

In the inverted microstrip region of the cell, the LC also contributes to the insertion loss; however, the LC absorption is very small. To estimate the amount of loss coming from the LC material, a drop of LC2020 is dispersed onto CPW and *S*-parameter measurements are taken. The results are then compared with measurements performed on the CPW without LC. As mentioned above, the LC2020 and LC1917 belong to the same family of LCs and therefore share many of the same chemical constituents [18]. Figure 6 shows the change in insertion loss ΔS_{21} vs frequency when a drop of LC is placed on top of CPW.

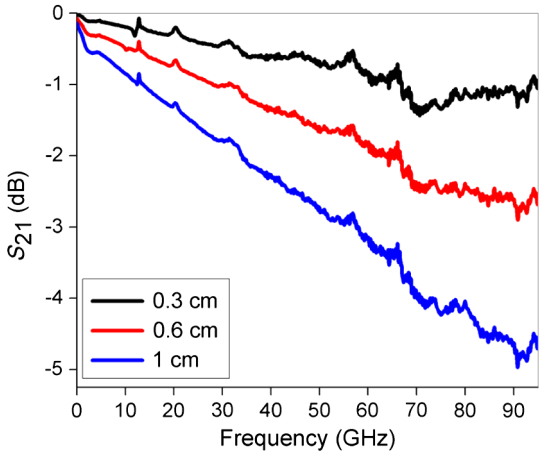

FIG. 5. S_{21} vs frequency of 2.25-μm-thick copper-based CPW structures on Borofloat 33 glass substrate.

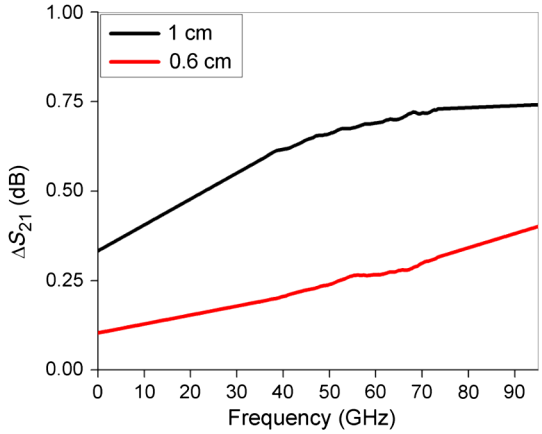

FIG. 6. The change in insertion loss ΔS_{21} vs frequency observed when a drop of LC material is placed on top of a CPW.

The 0.6- and 1-cm-long CPW are represented by the red and black curves, respectively. At 30 GHz, the 0.6 cm CPW exhibits 0.2 dB additional insertion loss when LC is placed on it. At the same frequency, a 1-cm CPW shows approximately 0.55 dB additional insertion loss from the LC. Comparing these S_{21} measurements (with and without LC material on top of the CPW) with S_{11} (not shown) leads to the conclusion that the absorption in LC is indeed small. Using a simple calculation, we determine that the loss tangent δ is approximately 0.005.

B. *S*-parameter characterization of a 30-GHz bandpass filter

As mentioned in the previous section, filters with passband frequencies of 30, 50, and 85 GHz are manufactured and on-wafer characterization is carried out using the VNA. The filter structures are filled with LC1917 to form a 38-μm-thick LC layer. For a 30-GHz bandpass filter with three stubs, the central frequency as a function of applied voltage is shown in Fig. 7(a), while the inset shows the changes of S_{21} vs frequency biased at various ac voltages. The passband central frequency is tuned from 32.3 to 29.2 GHz by varying the applied ac bias signal from 0 to 30 V p.p. across the LC layer. This corresponds to 10.3% tuning referenced to the design frequency of 30 GHz. Note that the onset of tuning occurs at 2 V p.p., which corresponds to the Fréedericksz transition [33]. Such behavior is observed for all built filters because the thickness of the LC layer is the same for all structures. The transition is associated with the value of the electric field needed to start the rotation of the LC molecules from the anchoring position. The majority of the tuning occurs between 2 and 14 V p.p. The passband width, defined as the frequency range over which the insertion loss is smaller than 50% of maximum power in the passband region, is 5 GHz. We note that the width of the passband region can be controlled by the width of the stubs [20,26].

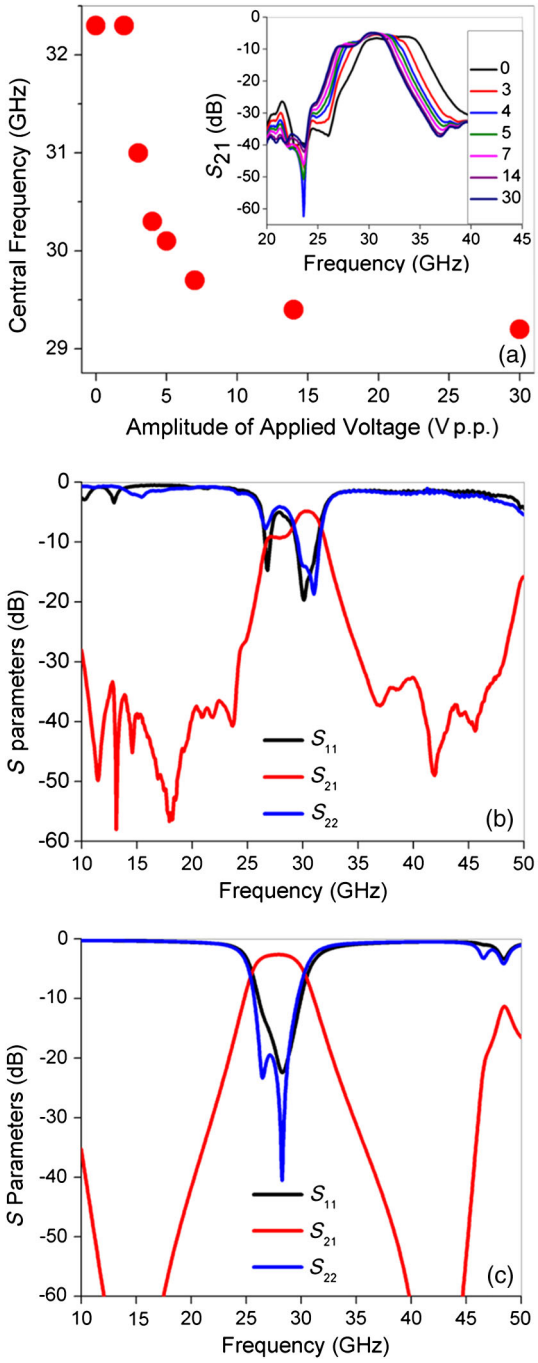

FIG. 7. Performance of a three-stub, 30-GHz bandpass filter. (a) Central frequency as a function of applied voltage. Inset shows transmission S_{21} vs frequency at various applied voltages. (b) A graph of S_{11}, S_{22}, and S_{21} vs frequency at 30 V p.p. (c) The results of CST simulation of S_{11}, S_{22}, and S_{21} vs frequency.

The Q factor of this filter is equal to 6. All of the filters reported in this study had approximately the same Q factor.

Figure 7(b) shows a graph of the reflection parameters S_{11} and S_{22} as well as transmission S_{21} vs frequency when the filter is biased with 30 V p.p. The transmission parameter in the pass region is not flat. Visible ripples in the transmission indicate the presence of multiple

reflections from CPW to microstrip transitions or glue regions, indicating the entire measured structure is not perfectly matched to 50 Ω. In the passband region, the insertion loss reaches −4.9 dB. The passband return loss ranges from −5 to −20 dB. The reflection parameters also overlap each other, indicating good alignment of the top ground plane with the bottom substrate supporting the signal line elements. Since the LC cell has 4 mm of excess CPW and 2.62 mm of excess microstrip-LC outside the filter structure, −1.3 dB of the insertion loss can be accounted for in the passband region of the filter.

The experimental results show reasonable agreement with simulations. A model of a 30-GHz filter with the same dimensions as the measured filter is created in CST Microwave Studio. The model excluded the CPW and CPW-microstrip transitions on the input and output of the filter. Figure 7(c) shows a CST simulation of S_{21} and S_{11} vs frequency of the filter with $\epsilon_{\parallel} = 3.7$, corresponding to the LC molecules being fully aligned with the electric field. There is a clearly defined peak in S_{21} at 30 GHz, with poles located at around 15 and 45 GHz. The passband width is roughly 5 GHz. Because the simulation neglects the CPW and transition region, the passband insertion loss is at −1.5 dB. Two resonances appear in the passband of the reflection parameters, resembling the experimental results.

As a final note concerning the physical 30-GHz filter devices, we would like to mention that the filters demonstrate good power handling. By introducing a 30-dB amplifier between the filter device and the first port of the VNA in the setup described in Sec. II, signals with power from 0.1 to 240 mW between 20–45 GHz are injected into the filter. The output power of the signal leaving the filter is linearly proportional to the input power. The LC media do not show any unwanted, nonlinear behavior while encountering an increase in signal power in the measured range. The same behavior is also expected for the higher-frequency filters described in the sections following. Similar power handling is observed for phase-shifter structures filled with the similar LC, W1825, up to 1 W of rf power in past research [9]. Finally, as far as total device power consumption is concerned, no more than 0.5 mW of power is needed to bias the LC-based filter devices.

C. *S*-parameter characterization of a 50-GHz bandpass filter

Figure 8(a) shows the passband central frequency as a function of applied voltage while the inset shows the transmission S_{21} vs frequency at various applied voltages for a 50-GHz filter. The passband central frequency is tuned from 52.7 to 47.6 GHz (10.3% tuning) by applying a 1-kHz, 0–30 V p.p. ac bias signal across the LC layer. The passband width is approximately 9 GHz. The inset shows that with increasing voltage, the transmission slowly gets better, indicating an improving match of the whole system to 50 Ω impedance.

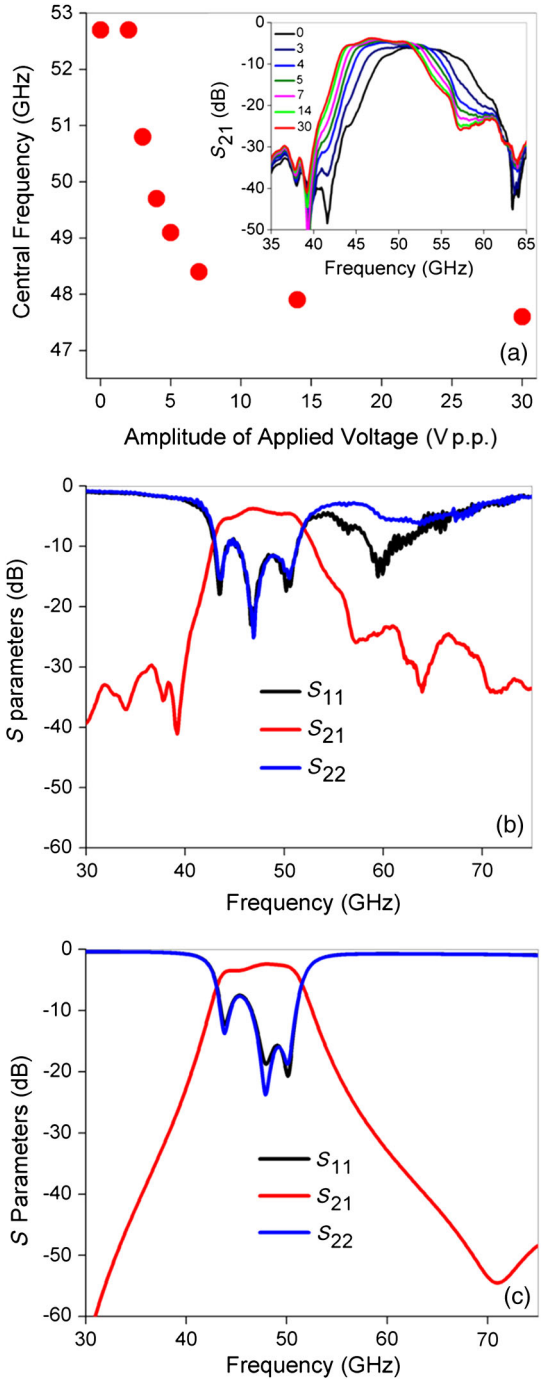

FIG. 8. Performance of a three-stub, 50-GHz bandpass filter. (a) Central frequency as a function of applied voltage. The inset shows transmission S_{21} vs frequency at various applied voltages. (b) A graph of S_{11}, S_{22}, and S_{21} vs frequency at 30 V p.p. (c) The results of CST simulation of S_{11}, S_{22}, and S_{21} vs frequency.

Figure 8(b) shows a graph of S_{11}, S_{22}, and S_{21} vs frequency at 30 V p.p. The transmission parameter S_{21} achieves −3.76 dB in the passband (the best value out of the three filters measured). The 50-GHz filter had 4 mm of excess CPW and 2.69 mm excess microstrip-LC, thus −1.8 dB of insertion loss may be accounted for. The

passband return loss ranges from −10 to −25 dB. The reflection parameters S_{11} and S_{22} also have a better overlap than observed for the 30-GHz filter, indicating very good alignment. The experimental results show good agreement with CST simulations. Figure 8(c) shows the simulation results for a 50-GHz filter. The passband insertion loss achieves −1.92 dB in the passband and peaks at 50 GHz, with poles around 25 and 75 GHz. Its passband width is approximately 9 GHz. We note that there is also a double resonance seen in the passband return loss, indicating a nonideal impedance match. However, insertion losses measured and predicted by CST simulations for this filter nearly match (−1.96 vs −1.92 dB). The passband region can be improved by further optimizing the filter dimensions.

D. *S*-parameter characterization of an 85-GHz bandpass filter

Figure 9(a) shows the passband central frequency as a function of applied voltage while the inset shows the transmission S_{21} vs frequency at various applied voltages for a three-stub, 85-GHz bandpass filter. The center passband frequency is tuned from 89.5 to 80.7 GHz (10.4% tuning) when a 1-kHz, 30-V-p.p. bias signal is applied. The passband width is 14 GHz. In Fig. 9(b), a graph of measured S_{11}, S_{22}, and S_{21} parameters vs frequency at 30 V p.p. bias is shown. The insertion loss reaches −7.63 dB in the passband region. With 4 mm excess CPW and 3.33 mm excess microstrip-LC, the −2.3 dB insertion loss is accounted for. The passband return loss ranges from −10 to −27 dB. Finally, a simulation of S_{21} and S_{11} vs frequency is performed on a filter with similar dimensions [see Fig. 9(c)]. The passband insertion loss reaches a value of −3.35 dB and is centered at 85 GHz, with a passband width of 14 GHz. Poles are located near 60 and 105 GHz. The passband return loss reaches −25 dB. The measured performance of the 85-GHz filter is in reasonable agreement with CST simulations, as one can see comparing Figs. 9(b) and 9(c).

E. Simulations of filters with three, five, and seven stubs

In the previous sections, we present results of CST simulations of three open-stub filters and compare them with experimental data. While the performance of these filters is close to the simulated results, we investigate the possibility of further performance improvements of filters shown in Fig. 1. We determine that a larger number of stubs can be implemented to improve the performance of the filters. Simulations indicate that with an increasing number of stubs, the insertion-loss magnitude in the passband region slightly increases, from −1.3 dB for three stubs to −2.8 dB with seven stubs, but with a significant increase in the roll-off. Figure 10, for example, shows simulations of S_{11} vs frequency of filters comparing three (black curve), five (red curve), and seven (blue curve) stubs, with a central

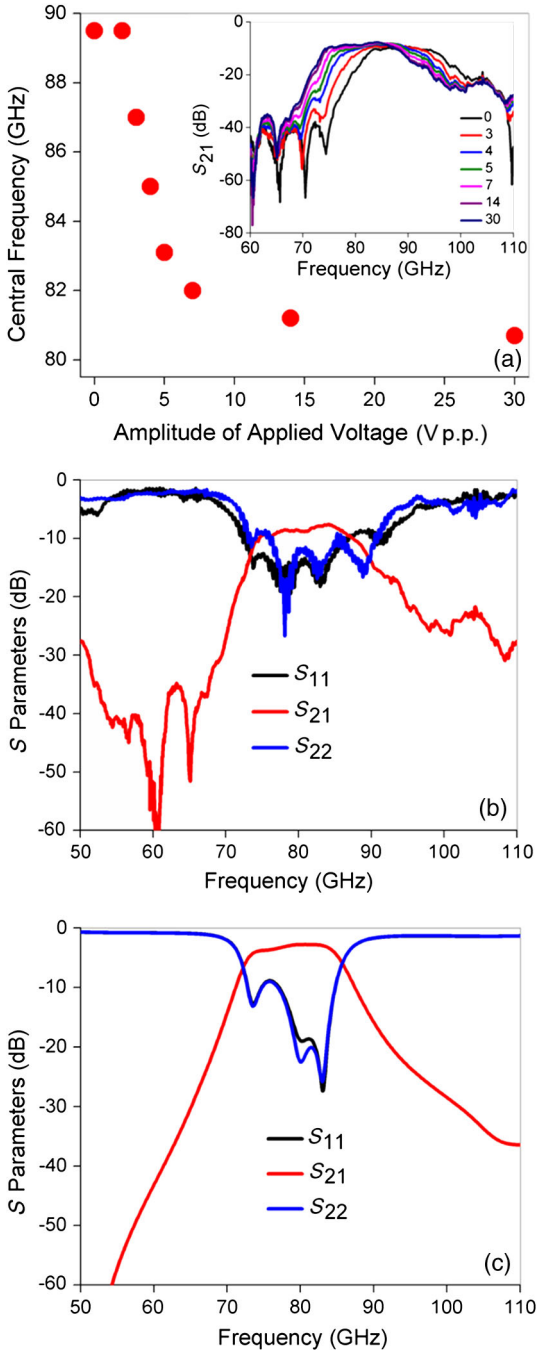

FIG. 9. Performance of a three-stub, 85-GHz bandpass filter. (a) Central frequency as a function of applied voltage. Inset shows transmission S_{21} vs frequency at various applied voltages. (b) A graph of S_{11}, S_{22}, and S_{21} vs frequency at 30 V p.p. (c) The results of CST simulation of S_{11}, S_{22}, and S_{21} vs frequency.

frequency of 30 GHz. The filter with three stubs has a roll-off of 8.3 dB/GHz (149 dB/octave) for frequencies below the bandpass region. When the number of stubs is increased to five, the roll-off increases to 16.7 dB/GHz (300 dB/octave). The seven-stub filter gives the best roll-off at 26.6 dB/GHz (480 dB/octave). These results clearly indicate that the larger number of stubs significantly

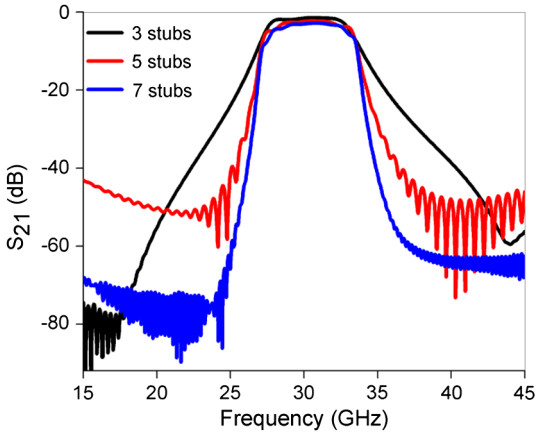

FIG. 10. S_{21} vs frequency of simulated filters with three (black curve), five (red curve), and seven (blue curve) stubs.

increases the filter performance. Other variations of the filter are also possible, including open-stub filters with a suppressed second harmonic [34]. We note that all these possible changes to filter construction (e.g., number of stubs) can be easily implemented in these LC-based microwave structures.

Comparing the CST simulation results with measured experimental structures indicates a very good agreement for roll-off values. We measure, for the three-stub 30-GHz filter, 180- and 140-dB/octave roll-off for frequencies below and above the passband region, respectively. Certain asymmetry is also visible in all CST simulated structures. For a 30-GHz filter, CST simulations predict 149 and 133-dB/octave roll-off for frequencies below and above the passband, respectively. The fact that the measured values of roll-off are better in the physical structure is attributed to the visible ripples in transmission as discussed in Sec. III B that enhance roll-off values for this particular filter. For the three-stub 50-GHz filter, the measured values of roll-off are 241 and 105 dB/octave for frequencies below and above the passband, respectively; from CST simulations these are 168 and 155 dB/octave, respectively. For the 50-GHz filter, the ripples in transmission skew the values of roll-off enhancing it for frequencies below the passband region and decreasing it for higher frequencies. A similar behavior is observed for the three-stub 85-GHz filter, where values of roll-off are 197 (168) and 93 (143) dB/octave below and above the measured (simulated) passband region, respectively.

IV. CONCLUSION

LC cells containing three-stub tunable bandpass filters in inverted microstrip geometry are designed, manufactured, and tested. The cells utilize a broadband CPW-microstrip transition for injection of the microwave and bias signals into the filter. Filters with various stub dimensions are designed to have center passband frequencies at 30, 50, and 85 GHz. The passband frequencies are tunable by at least 10% using a 1-kHz, 14 -V-p.p. ac bias signal. The electric field applied across the LC is less than 0.19 V/μm. The smallest insertion loss, seen in the 50-GHz filter, is −3.76 dB, which could be further reduced. The Q factor for all filters is approximately 6. The return loss of all three devices ranged from −10 to −25 dB, indicating a good impedance match for a proof-of-concept device. Furthermore, experimental results are in good agreement with the results from CST simulations performed on filters with identical dimensions. Losses due to the LC media are significantly smaller than 1 dB/cm from 1–110 GHz for the structures with dimensions presented in this paper.

The presented results of the proof-of-concept devices clearly indicate that the LC-based microwave and millimeter wave bandpass filters can operate over a wide range of frequencies due to the fact that there is little dispersion in the studied LC materials (constant group delay) [9]. It is the lack of resonances in the gigahertz frequencies that makes it possible to employ the same physical principles and technology to design and build bandpass filters operating at 30 as well as 90 GHz. Actually, we expect that devices in sub-THz frequencies can be realized. This opens, in our view, alternative opportunities to create tunable devices operating in frequencies up to hundreds of gigahertz.

Finally, the developed filter structures open an opportunity for studies of the fundamental properties of LC materials, far beyond their scope in the rf and microwave signal-processing applications. Since the primary passband resonance of the filters is dependent on the permittivity of the used LC, these devices offer a method for effectively determining the dielectric permittivity. In fact, multiple passband resonances, which are a normal feature of open-stub filters, allow one to determine the dispersion relation of LC materials over a wide range of frequencies. Moreover, only a small quantity of LC material is needed when compared with other methods mentioned previously. This alternative metrology for determination of dielectric properties is not just limited to LCs, but also to fluids or solid in general at sub-THz frequencies.

ACKNOWLEDGMENTS

The authors thank Dr. Dario Bueno-Baques and Olha Melnyk for help with the LC cell-assembly process and Natalie Bledowski for thin-film deposition.

[1] D. M. Pozar, *Microwave Engineering* (Wiley, New Jersey, 2012).
[2] D. B. Cruickshank, *Microwave Materials for Wireless Applications* (Artech House, Boston, 2011).
[3] J. L. Lovejoy Jr., Ph.D. dissertation, University of Colorado at Colorado Springs, 2012.
[4] O. H. Karabey, Ph.D. dissertation, Technische Universitat Darmstadt, 2014.

[5] J. Piotrowski, J. Parka, and E. Nowinowski-Kruszelnicki, Nematic liquid crystals in inverted microstrip structures, Proc. SPIE Int. Soc. Opt. Eng. **8902**, 89022B (2013).

[6] D. Dolfi, M. Labeyrie, P. Joffre, and J. P. Huignard, Liquid crystal microwave phase shifter, Electron. Lett. **29**, 926 (1993).

[7] K. C. Lim, J. D. Margerum, and A. M. Lackner, Liquid crystal millimeter wave electronic phase shifter, Appl. Phys. Lett. **62**, 1065 (1993).

[8] C. Weil, G. Luessem, and R. Jakoby, Tunable inverted-microstrip phase shifter device using nematic liquid crystals, IEEE MTT-S Int. Microwave Symp. Dig. **3**, 7308363 (2002).

[9] Y. Garbovskiy, V. Zagorodnii, P. Krivosik, J. Lovejoy, R. E. Camley, J. Dziaduszek, and R. Dąbrowski, Liquid crystal phase shifters at millimeter wave frequencies, J. Appl. Phys. **111**, 054504 (2012).

[10] P. G. de Gennes and J. Prost, *The Physics of Liquid Crystals* (Oxford University Press, New York, 1993).

[11] J. Baker-Jarvis, R. G. Geyer, J. H. Grosvenor, M. D. Janezic, C. A. Jones, B. Riddle, C. M. Weil, and J. Krupka, Dielectric characterization of low-loss materials a comparison of techniques, IEEE Trans. Dielectr. Electr. Insul. **5**, 571 (1998).

[12] F. Dubois, F. Krasinskj, B. Splingart, N. Tentillier, C. Legrand, A. Spadlo, and R. Dabrowski, Large microwave birefringence liquid-crystal characterization for phase shifter applications, Jpn. J. Appl. Phys. **47**, 3564 (2008).

[13] R. Kowerdziej, M. Olifierczuk, J. Parka, and J. Wróbel, Terahertz characterization of tunable metamaterial based on electrically controlled nematic liquid crystal, Appl. Phys. Lett. **105**, 022908 (2014).

[14] J. F. Bernigaud, N. Martin, P. Laurent, C. Quendo, G. Tanné, B. Della, F. Huret, and P. Gelin, in *Proceedings of the 36th European Microwave Conference, Manchester, U.K., 2006* (IEEE, New York, 2006).

[15] S. Missaoui and M. Kaddour, Liquid crystal-based reconfigurable tunable filter with DBR topology, ISRN Mater. Sci. **2011**, 784615 (2011).

[16] J. Torrecilla, V. Urruchi, J. M. Sánchez-Pena, N. Bennis, A. Garcia, and D. Segovia, Improving the pass-band return loss in liquid crystal dual-mode bandpass filters by microstrip patch reshaping, Materials **7**, 4524 (2014).

[17] F. Goelden, A. Gaebler, O. Karabey, M. Goebel, A. Manabe, and R. Jakoby, in *Proceedings of the German Microwave Conference, Berlin, 2010* (IEEE, New York, 2010).

[18] R. Dąbrowski, J. Dziaduszek, A. Ziółek, Ł. Szczuciński, Z. Stolarz, G. Sasnouski, V. Bezborodov, W. Lapanik, S. Gauza, and S. T. Wu, Low viscosity, high birefringence liquid crystalline compounds and mixtures, Opto-Electron. Rev. **15**, 1 (2007).

[19] R. Dąbrowski, P. Kula, and J. Herman, High birefringence liquid crystals, Crystals **3**, 3 (2013).

[20] G. L. Matthaei, L. Young, and E. M. T. Jones, *Microwave Filters, Impedance-Matching Networks, and Coupling Structures* (McGraw-Hill, New York, 1964).

[21] T. C. Edwards and M. B. Steer, *Foundations of Interconnect and Microstrip Design* (Wiley, New York, 2000).

[22] M. Barbuto, A. Alù, F. Bilotti, A. Toscano, and L. Vegni, Characteristic impedance of a microstrip line with a dielectric overlay, *COMPEL* 32, 6 (2013).

[23] J. V. Hughes and H. L. Armstrong, The dielectric constant of dry air, J. Appl. Phys. **23**, 501 (1952).

[24] U. Chodorow, E. Mavrona, N. Palka, O. Strzezysz, K. Garbat, S. Saitzek, J. F. Blach, V. Apostolopoulos, M. Kaczmarek, and J. Parka, Terahertz properties of liquid crystals doped with ferroelectric $BaTiO_3$ nanoparticles, Liq. Cryst. **44**, 1207 (2017).

[25] K. Kowiorski, J. Kędzierski, Z. Raszewski, M. A. Kojdecki, O. Chojnowska, K. Garbat, E. Miszczyk, and W. Piecek, Complementary interference method for determining optical parameters of liquid crystals, Phase Transitions **89**, 403 (2016).

[26] T. H. Lee, *Planar Microwave Engineering: A Practical Guide to Theory, Measurements, and Circuits* (Cambridge University Press, Cambridge, U.K., 2004).

[27] D. Chen, Q. Wang, and Z. Shen, in *Proceedings of the 2005 Asia-Pacific Microwave Conference Proceedings* (IEEE, New York, 2005).

[28] X. Zhang, B. Lee, C.-y. Lin, A. X. Wang, A. Hosseini, and R. T. Chen, Highly linear broadband optical modulator based on electro-optic polymer, IEEE Photonics J. **4**, 6 (2014).

[29] Y. G. Kim, K. W. Kim, and Y. K. Cho, in *2008 IEEE MTT-S International Microwave Symposium Digest* (IEEE, New York, 2008).

[30] R. H. Chen, *Liquid Crystal Displays: Fundamental Physics and Technology* (Wiley, Hoboken, 2011).

[31] J. E. Nobles, V. Zagorodnii, A. Hutchison, and Z. Celinski, Biasing vector network analyzers using variable frequency and amplitude signals, Rev. Sci. Instrum. **87**, 084701 (2016).

[32] D. C. DeGroot, J. A. Jargon, and R. B. Marks, in, *60th ARFTG Conference Digest, Fall 2002* (IEEE, New York, 2002).

[33] V. Fréedericksz and A. Repiewa, Theoretisches und experimentelles zur frage nach der natur der anisotropen flüssigkeiten, Z. Phys. **42**, 532 (1927).

[34] W-H. Tu and K. Chang, Compact second harmonic-suppressed bandstop and bandpass filters using open stubs, IEEE Trans. Microwave Theory Tech. **54**, 2497 (2006).